Martin Schmid · Andreas Lorke · Alfred Wüest
Michel Halbwachs · Gregory Tanyileke

Development and sensitivity analysis of a model for assessing stratification and safety of Lake Nyos during artificial degassing

Abstract To prevent the recurrence of a disastrous eruption of carbon dioxide (CO_2) from Lake Nyos, a degassing plan has been set up for the lake. Since there are concerns that the degassing of the lake may reduce the stability of the density stratification, there is an urgent need for a simulation tool to predict the evolution of the lake stratification in different scenarios. This paper describes the development of a numerical model to predict the CO_2 and dissolved solids concentrations, and the temperature structure as well as the stability of the water column of Lake Nyos. The model is tested with profiles of CO_2 concentrations and temperature taken in the years 1986 to 1996. It reproduces well the general mixing patterns observed in the lake. However, the intensity of the mixing tends to be overestimated in the epilimnion and underestimated in the monimolimnion. The overestimation of the mixing depth in the epilimnion is caused either by the parameterization of the k-epsilon model, or by the uncertainty in the calculation of the surface heat fluxes. The simulated mixing depth is highly sensitive to the surface heat fluxes, and errors in the mixing depth propagate from one year to the following. A precise simulation of the mixolimnion deepening therefore requires high accuracy in the meteorological forcing and the parameterization of the heat fluxes. Neither the meteorological data nor the formulae for the calculation of the heat fluxes are available with the necessary precision. Consequently, it will be indispensable to consider different forcing scenarios in the safety analysis in order to obtain robust boundary conditions for safe degassing. The input of temperature and CO_2 to the lake bottom can be adequately simulated for the years 1986 to 1996 with a constant sublacustrine source of $18 \, l \, s^{-1}$ with a CO_2 concentration of $0.395 \, mol \, l^{-1}$ and a temperature of 26 °C. The results of this study indicate that the model needs to be calibrated with more detailed field data before using it for its final purpose: the prediction of the stability and the safety of Lake Nyos during the degassing process.

Keywords Lake Nyos · k-epsilon model · Crater lakes · Lake degassing · Heat balance · Carbon dioxide

M. Schmid (✉) · A. Lorke · A. Wüest
EAWAG, Seestrasse 79,
6047 Kastanienbaum, Switzerland
e-mail: martin.schmid@eawag.ch
Tel.: ++41 41 349 21 93
Fax: ++41 41 349 21 62

M. Halbwachs
Université de Savoie, BP 1104, Savoie Technolac,
73376 Le Bourget du Lac Cedex, France

G. Tanyileke
Institute for Geological and Mining Research (IRGM),
4110 Yaoundé, Cameroon

1 Introduction

Lake Nyos has had an infamous reputation since August 1986, when it released a large cloud of carbon dioxide (CO_2), which flowed down the neighbouring valleys and asphyxiated 1700 people (Kling et al. 1987). With the exception of a similar gas burst of smaller scale at nearby Lake Monoun (Sigurdsson et al. 1987), this volcanological hazard had not been previously known. The disaster was followed by an intense scientific discussion about the origin of the gas burst. According to the limnic eruption hypothesis, high CO_2 concentrations had slowly built up in the lake water column, and a large part of the CO_2 was released after a trigger mechanism led to local supersaturation. The exact nature of the trigger mechanism remains unknown, but if the CO_2 concentrations had been near saturation below the chemocline, a baroclinic displacement could have led to local supersaturation and triggered a self-amplifying plume (Evans et al. 1994). The slow recharge of CO_2 to the bottom water of the lake, observed after the eruption (Evans et al. 1994; Kusakabe et al. 2000; Nojiri et al. 1993), strongly supports this hypothesis, even though it

seems to contradict some eye-witness accounts (Leguern et al. 1992). Our work therefore is based on the limnic eruption hypothesis. Nevertheless, it should be kept in mind that sudden volcanic activity leading to similar disasters cannot be excluded in this region.

Lake Nyos is one of several crater lakes in the northwestern part of Cameroon (Kling 1988). The lake is situated 1091 m asl and has a surface area of 1.58 km^2, a volume of 0.15 km^3 and a maximal depth of 208 m (Nojiri et al. 1993). The water column of the lake can be divided into three distinctly different sections which are separated from each other by two chemoclines at 50 and 170 m depth (Fig. 1). Seasonal mixing reaches only the top 50 m, the *mixolimnion*, where the CO_2 concentrations have decreased since the eruption because of the exchange with the atmosphere. In the *hypolimnion* between 50 and 170 m depth, temperatures and CO_2 concentrations have remained almost unchanged since the eruption, and the almost linear increase of temperature and conductivity with depth, observed after the eruption, is still prominent. In the *monimolimnion* from 170 to 208 m depth, CO_2 concentrations and temperature have strongly increased since 1986.

Because the rebuilding of high CO_2 concentrations in the water column could lead to a new disaster within decades, a plan was set up to degas the lake (Kling et al. 1994). In January 2001, after several experimental tests in preceding years, a first polyethylene pipe was installed in Lake Nyos (Halbwachs 2002; Halbwachs and Sabroux 2001). Water is withdrawn at a depth of 203 m and discharged as a fountain on the lake surface. Due to
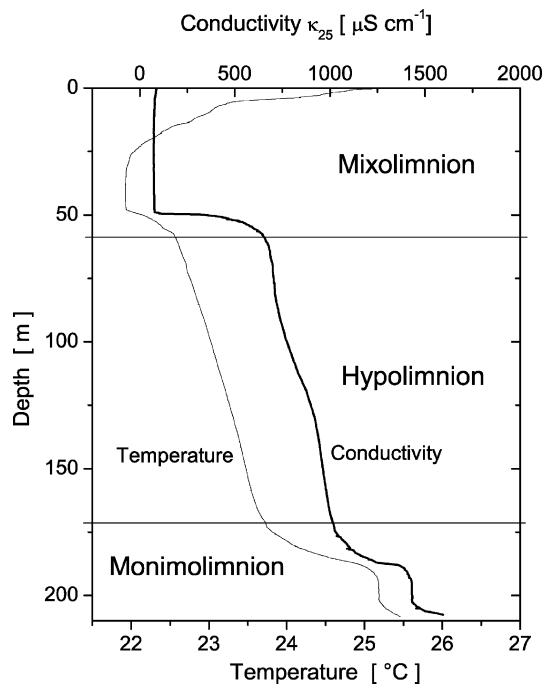
the high CO_2 pressure in the monimolimnion, the water flow through the tube is self-sustaining, driven by the expansion of the generated bubbles. A detailed description of the degassing procedure can be found on the Lake Nyos degassing homepage (Halbwachs 2002).

However, there is concern that the degassing procedure could lower the stability of the stratification by lifting heavy bottom water to the surface, and thus impose the risk of a future eruption (Pickrell 2001). The aim of this study is to develop a simulation model that can be used to assess the safety of different degassing scenarios, including the sensitivity of the system to the forcing parameters, for Lake Nyos, and with adapted initial and boundary conditions also for Lake Monoun.

Previous simulation results have suggested that the stratification below the mixolimnion should remain stable during the degassing process (McCord and Schladow 1998), and that a new eruption is more likely to be caused by destratification leading to local supersaturation in the monimolimnion than by deep mixing from the surface (Kantha and Freeth 1996). Compared to these simulations, our model features the following important additions:

1. The meteorological forcing varies from year to year and is inferred from the best available observed data. The variable meteorological forcing makes it possible to demonstrate its strong influence on the mixing processes in the lake.
2. The geochemical cycling is more completely represented in the model. The bottom water of Lake Nyos contains large amounts of dissolved reduced iron and other minerals. Transported to the surface, the iron is oxidized and transformed to amorphous iron hydroxide particles (Davison 1993). The iron particles increase the density in the surface water and – after sedimentation and reduction to Fe^{2+} – also below the oxycline. Furthermore, they increase the light absorption at the surface and thus reduce the penetration depth of solar irradiation. Since the lake surface is usually near its equilibrium temperature, the heat input from solar radiation is approximately balanced by heat losses at the lake surface. Consequently, the heat balance directly at the surface is negative, which leads to a convectively mixed surface layer. This convective mixing is reduced by stronger light absorption in the surface layer.
3. In addition to the standard k-epsilon model, turbulent energy is also transferred from the wind stress via internal seiches to the hypolimnion. It has been shown that this mixing can contribute significantly to diapycnal transport in lakes (Gloor et al. 2000).

The present paper describes the model development, the comparison of simulations with historical data and the sensitivity analysis. These are important steps to improve our understanding of the simulated system. The results of this study show that the model is applicable for the simulation of mixing processes in Lake Nyos, but that more field data are needed for the detailed model

Fig. 1 Temperature and conductivity at 25 °C observed in Lake Nyos in November 2001, and definition of the three distinctively different layers in the lake

calibration. A mooring was installed in the lake in November 2001 to collect the necessary additional data. The data from the mooring, together with new CTD profiles, will be used to calibrate the model in greater detail. This final version of the model will be used to simulate the stratification in the lake for different degassing scenarios, to analyze the risk of a CO_2 eruption for these scenarios, and to draw recommendations for the optimization of the degassing procedure.

2 Model description

We developed a vertical one-dimensional model of Lake Nyos with a resolution of 0.5 m. The model was implemented within the lake module of the software AQUASIM 2.1 (Reichert 1994, 1998), which is designed to concurrently simulate physical and biogeochemical processes in natural and technical aquatic systems. AQUASIM uses the DASSL algorithm (Petzold 1983), in which the time step and the integration order are constantly adapted following the evaluation of convergence criteria. The simulation is driven by daily (cloud cover, vapour pressure, irradiation and wind speed) and monthly (temperature and precipitation) weather data. Figure 2 gives an overview of the main model processes described in detail in the following chapters. The notation, units and parameter values are summarized in Table 1. Some of the equations given below are empirical and only valid with the units given in Table 1.

Fig. 2 Schematic overview of the Lake Nyos simulation model. The notation is explained in Table 1
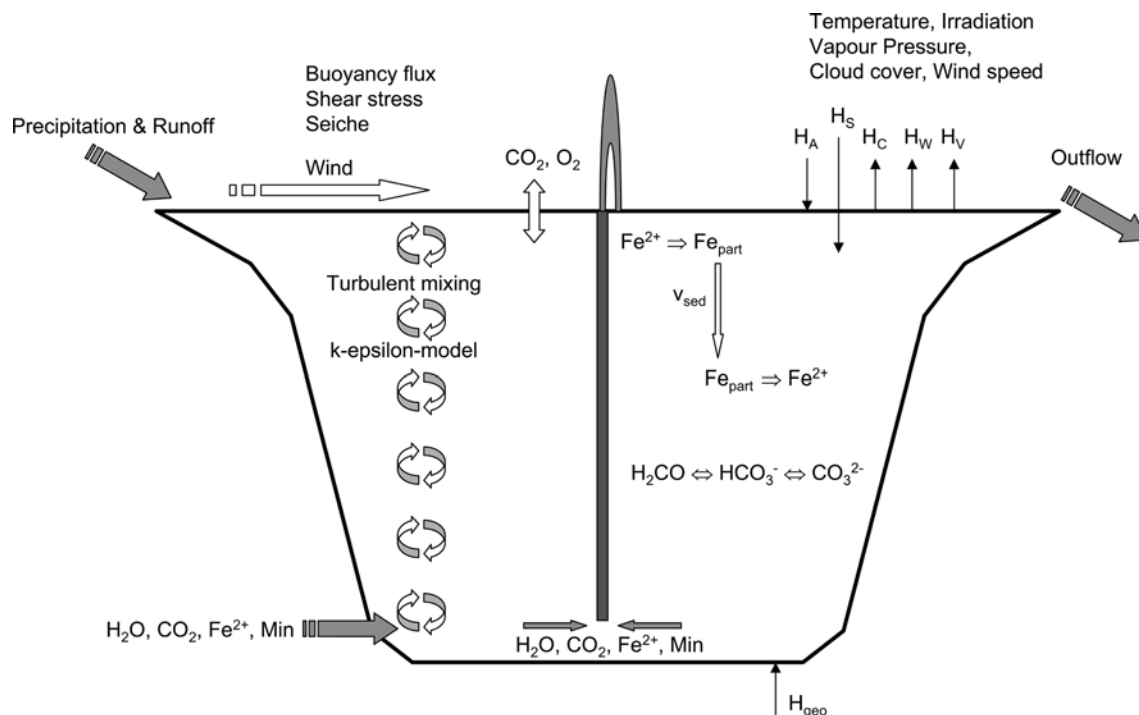
2.1 Water balance

The net water inflow at the surface is estimated as the difference between precipitation and evaporation E_P (Eq. 9), in the lake catchment area of 7.2 km². The inflow is set to zero if evaporation exceeds precipitation, which is generally the case during the dry season from mid-November to February. The average net water inflow at the surface is 0.35 m³ s⁻¹. Another water input is located in the monimolimnion, which is considered to be the source for the observed increasing mineral concentrations and temperatures in this layer (Kusakabe et al. 2000). The lake surface elevation is assumed to be constant in the model by closing the water balance with the surface outflow. In reality the lake level drops by ca. 2 m in the dry season (Evans et al. 1994). The difference is not critical for the conclusions of this study, as it is only 1% of the lake depth. The degassing of the lake is simulated by removing water at the intake depth z_{in} of the degassing pipe and introducing the degassed water at the lake surface. The water flow through the degassing pipe is parameterized depending on the intake depth and the partial pressure of CO_2 at z_{in}. The currently installed pipe has an intake depth of 203 m, a diameter of 14.5 cm and a water flow of 65 l s⁻¹ (M. Halbwachs, personal communication).

2.2 Meteorological forcing

The results presented below show a high sensitivity of the model to the heat fluxes at the lake surface and consequently to the meteorological forcing. They are the main factors determining the development of the stratification in the top 100 m of the water column during the

Table 1 Notation and units

A	cross-sectional area of the lake water column	m^2
A_B	area of the lake bottom boundary	m^2
Alk	alkalinity (calculated from alkali metal concentrations)	mol m^{-3}
B	buoyancy flux	W kg^{-1}
Bowen	Bowen ratio, corrected for altitude	0.567 mbar K^{-1}
C	cloud cover	–
C_D	bottom friction coefficient	0.002
c_I	transmissivity of the atmosphere without clouds	0.69
$[CO_2]$	total concentration of carbon dioxide (including HCO_3^- and CO_3^{2-})	mol m^{-3}
$c3_{TKE}$	parameter in the dissipation equation of the k-epsilon model	$B > 0$: 1.0, $B < 0$: −0.4
e_A	vapour pressure	mbar
E_A	atmospheric infrared emission coefficient	–
E_P	evaporation	m s^{-1}
e_S	saturated vapour pressure at lake surface temperature	mbar
E_{seiche}	integrated energy content of the seiche	J
$[Fe]$	concentration of dissolved iron (Fe^{2+})	mol m^{-3}
$[Fe_{Part}]$	concentration of particulate iron	mol m^{-3}
H_A	incoming infrared radiation from atmosphere	W m^{-2}
H_C	sensible heat flux	W m^{-2}
H_{geo}	geothermal heat flux	0.1 W m^{-2}
H_S	solar radiation penetrating the water surface	W m^{-2}
H_V	latent heat flux	W m^{-2}
H_W	outgoing infrared radiation from water surface	W m^{-2}
I_{ext}	solar radiation at the top of the atmosphere	W m^{-2}
I_{tot}	incoming solar radiation at the water surface	W m^{-2}
$K_{\lambda Fe}$	coefficient for the estimation of light absorption due to Fe particles	94 m^2 kg^{-1}
L_W	evaporation heat of water (at 25 °C)	2.442×10^6 J kg^{-1}
M_{CO_2}	molar mass of CO_2	0.044 kg mol^{-1}
M_{Fecarb}	molar mass of $Fe(HCO_3)_2$	0.1779 kg mol^{-1}
M_{FePart}	molar mass of $Fe(OH)_3$	0.1069 kg mol^{-1}
M_{HCO_3}	molar mass of HCO_3^-	0.0610 kg mol^{-1}
Min	total concentration of alkali metals	kg m^{-3}
$[O_2]$	oxygen concentration	mol m^{-3}
$p1, p2$	sensitivity parameters for H_A and H_V	1
P_{seiche}	turbulent kinetic energy production by the seiche	W kg^{-1}
r_A	reflection of infrared radiation at lake surface	0.03
r_S	reflection of solar radiation at lake surface (Eq. 9)	–
T	temperature (with circumflex: absolute temperature)	°C (K)
T_{air}	air temperature	°C
T_{surf}	water temperature at lake surface	°C
u_{10}	wind speed 10 m above lake surface	m s^{-1}
z	vertical coordinate	m
β_{CO_2}	contraction coefficient of carbon dioxide (Ohsumi et al. 1992)	2.84×10^{-4} m^3 kg^{-1}
β_{Fe}	contraction coefficient of dissolved iron carbonate	8.38×10^{-4} m^3 kg^{-1}
β_I	fraction of incoming solar radiation absorbed at the water surface	0.4
β_{Min}	average contraction coefficient of dissolved alkali carbonates	7.89×10^{-4} m^3 kg^{-1}
β_{Part}	contraction coefficient of $Fe(OH)_3$ particles with a density of 2800 kg m^{-3}	6.40×10^{-4} m^3 kg^{-1}
γ	coefficient for seiche energy decay	6.2×10^{-11} kg$^{-1/2}$ m^{-1}
λ	light absorption coefficient of Lake Nyos water with Fe particles	m^{-1}
λ_0	light absorption coefficient of Lake Nyos water without Fe particles	0.4 m^{-1}
ρ	water density	kg m^{-3}
ρ_W	constant approximation of water density	997.5 kg m^{-3}
σ	Stefan-Boltzmann constant	5.67×10^{-8} W m^{-2} K^{-4}

10 years of simulation. For this reason, great care was taken to extract a reasonable set of meteorological forcing from the available data. On the other hand, the sensitivity is so high that it is hardly possible to estimate the heat fluxes with sufficient precision from the available data, and even less to predict them for future safety analyses; but even though the meteorological forcing and the heat fluxes have a strong effect on the results of the simulations, they are not critical for the main conclusions of this study.

The local climate consists of a shorter dry season from November to February with a daily precipitation of less than 2 mm, and a longer wet season with generally two precipitation maxima in April/May and August/September. No direct measurements of the meteorological forcing were available for the simulation time of 1986 to 1996. The data used were inferred from the following data sources:

2.2.1 Incoming shortwave radiation

The extraterrestrial shortwave radiation I_{ext} was calculated according to Eqs. (A1), (A2) and (A3) in

Henderson–Sellers (1986). The shortwave radiation penetrating the lake surface was calculated using Eqs. (1) and (2).

$$I_{tot} = I_{ext} \cdot c_I \cdot (1 - 0.65 \cdot C^2) \tag{1}$$

$$H_S = I_{tot} \cdot (1 - r_S) \ , \tag{2}$$

where C is the cloud cover, and c_I is the transmissivity of the atmosphere without clouds estimated for Accra in Ghana (Davies 1965, cited in Brutsaert 1982), and increased by 0.02 because of the high altitude of the lake. The empirical Eq. (3) was used to estimate r_S, the reflection of shortwave radiation at the lake surface (Dingman et al. 1967, cited in Henderson–Sellers 1986).

$$r_S = 0.108 - 0.000139 \cdot I_{tot} \ . \tag{3}$$

Forty percent of the solar radiation is absorbed at the lake surface (Henderson–Sellers 1986); the rest penetrates into the epilimnion with an attenuation coefficient that increases linearly with the particulate iron concentration (Eq. 4).

$$\lambda = \lambda_0 + k_{\lambda Fe} \cdot [Fe_{part}] \cdot m_{FePart} \ . \tag{4}$$

The absorption coefficient of Lake Nyos water without particulate iron, λ_0, was estimated at 0.4 m^{-1} (Kling 1988; Kling et al. 1989), the dependence of the light absorption on particulate iron concentrations $k_{\lambda Fe}$ was inferred from data for suspended particulate matter (Gallegos and Moore 2000). The uncertainty of this parameter is high, as the light absorption depends on the size distribution of the particles.

2.2.2 Vapour pressure, cloud cover and wind speed

Daily data was extracted from the data of the NOAA NCEP-NCAR CDAS-1 reanalysis project (Kalnay et al. 1996). The wind speed was multiplied with a constant factor of 1.74 to adjust to the average wind speed of 2.4 m s^{-1} as observed in 1989 at the lake (McCord and Schladow 1998). The vapour pressure was corrected for altitude. The wind speed reaches a maximum in March with average wind speeds of 3–4 m s^{-1}. The minima of cloud cover and vapour pressure in the dry season show large interannual variation.

2.2.3 Air temperature

The monthly mean temperature data for Cameroon (Mitchell et al. 2002) were corrected to fit the long-term monthly averages of the meteorological station in Ko-undja, situated 100 km southeast of the lake (NOAA NCDC monthly station dataset). An offset of 0.8 °C was added to the resulting value, because the station is situated 120 m above the lake surface. The average temperature is very constant throughout the year, ranging from 20 to 24 °C, with highest temperatures at the transition between the dry and the wet season.

2.2.4 Precipitation

Monthly precipitation was obtained from the Global Precipitation Climate Project data (Huffman et al. 1997). These data were available for 1987 to mid-1996. For the few remaining months the monthly averages for Cameroon (Mitchell et al. 2002) were used. The average annual precipitation is 2.6 m.

2.2.5 Diurnal variation

Since only daily averages of the meteorological forcing were used as model input, the diurnal variation is neglected. Consequently, the stratification during the day and the mixing in the night caused by the diurnal variation of solar irradiation cannot be reproduced by the model. However, model runs over a year with the diurnal cycle of solar irradiation included have shown no significant difference in the long-term development of the stratification. The same result was obtained with an artificially introduced diurnal wind variation. Since the computation speed was considerably reduced by the diurnal variation and the available data were not sufficient to produce a realistic wind time series with high temporal resolution, it was decided to perform the simulations with average daily data.

2.3 Heat balance

The heat exchange between the lake surface and the atmosphere includes short-wave (H_S, Eqs. 1 and 2) and infrared radiation from the atmosphere (H_A, Eq. 5), infrared radiation from the water surface (H_W, Eq. 7), latent heat flux (H_V, Eq. 8) and sensible heat flux (H_C, Eq. 10) with positive heat fluxes directed from the atmosphere to the lake (Goudsmit et al. 2002; Henderson–Sellers 1986; Imboden and Wüest 1995).

$$H_A = p_1 \cdot (1 - r_A) \cdot E_A \cdot \sigma \cdot \hat{T}_{air}^4 \ , \tag{5}$$

$$E_A = 1.24 \cdot (1 + 0.17 \cdot C^2) \cdot \left(\frac{e_A}{\hat{T}_{air}}\right)^{1/7} \ , \tag{6}$$

$$H_W = -0.97 \cdot \sigma \cdot (\hat{T}_{surf})^4 \ , \tag{7}$$

$$H_V = -p_2 \cdot (e_S - e_A)$$
$$[4.4 + 1.82 \cdot u_{10} + 0.26 \cdot (T_{surf} - T_{air})] \ , \tag{8}$$

$$E_P = -\frac{H_V}{\rho_W \cdot L_W} \ , \tag{9}$$

$$H_C = Bowen \cdot H_V \cdot \frac{(T_{surf} - T_{air})}{(e_S - e_A)} \ . \tag{10}$$

There is a large variety of equations available for the estimation of these heat fluxes, especially for the H_V, H_C and I_{tot} (Henderson–Sellers 1986). Choosing another equation may easily result in a difference of 20–50 W m^{-2} in the heat flux estimates. An additional
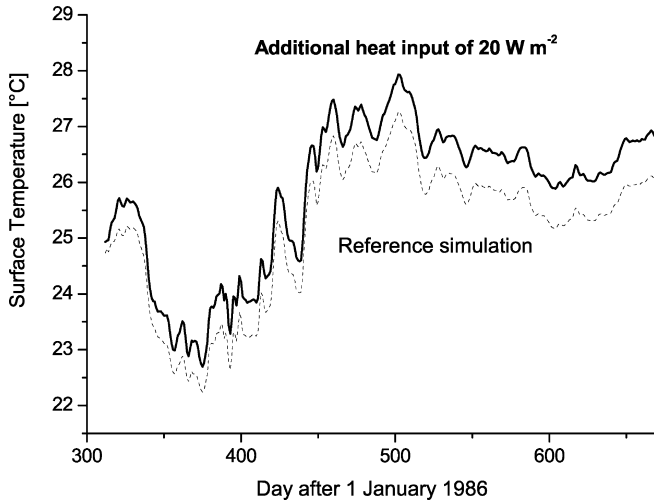
Fig. 3 Simulated surface temperature from November 1986 to November 1987 in the reference simulation (*dotted line*) and with an additional heat input to the lake surface of 20 W m^{-2} (*solid line*)

heat input of 20 W m^{-2} will typically increase the lake-surface temperature by about 0.7 °C (Fig. 3).

Further heat inputs to the water column are the sub-lacustrine source and the geothermal heat flow from the sediment H_{geo}, which was chosen to 0.1 W m^{-2}, the upper limit of terrestrial heat flows observed in West Africa (Lucazeau et al. 1991). The temperature of the water passing through the degassing pipe is lowered by 1 °C per 210 mmol l^{-1} CO_2 due to the exsolution heat of CO_2 of 20 kJ mol^{-1}.

2.4 Turbulent mixing

The physical mixing of the lake is simulated with a buoyancy-extended k-epsilon turbulence model (Goudsmit et al. 2002). Turbulent mixing is driven by the energy introduced into the system by surface shear stress from wind forcing, and by buoyancy due to heat loss to the atmosphere or heat input to the monimolimnion. In addition to standard k-epsilon models, this model includes energy transfer from the wind via internal seiches to turbulent kinetic energy in the bottom boundary layer. It has been shown that this mixing can contribute significantly to diapycnal transport in lakes (Gloor et al. 2000). To avoid numerical problems, the upper limit of the turbulent diffusion coefficient was set to 0.1 m^2 s^{-1}, which is sufficient to mix a layer of 10 m within 10 min. The water density ρ is calculated with the equation of state (Eq. 11), depending on temperature and on the concentrations of carbon dioxide, dissolved alkali metals (Min) and dissolved and particulate iron.

The equation of state contains the following simplifications and assumptions: the haline contraction coefficients β_i are assumed to be constant. Since bicarbonate is almost the only negative ion in the water column (Kusakabe et al. 2000), it is assumed that all positive ions are actually dissolved bicarbonate salts. The relative composition of the minerals except Fe is assumed constant. The haline contraction coefficient β_{Min} was calculated with the method developed by Wüest et al. (1996) for Lake Malawi.

Compared to the model described by Goudsmit et al. (2002), the version implemented in AQUASIM 2.1 is simplified in the following points: only one velocity direction is considered, and consequently the effect of the Coriolis force is neglected. The effect of the Coriolis force can be assumed negligible, because of the proximity to the equator and the small size of the lake. However, since the wind stress is always in the same direction and the currents are not deflected by the Coriolis force, a counter pressure term proportional to the current velocity was included in the momentum equation to avoid the buildup of unrealistically strong currents. The simulation results are not sensitive to the value of the proportionality constant. Finally, the transfer of seiche energy to turbulent kinetic energy depends only on the bathymetry of the lake, but not on the stability of the water column. Equation (12) is used for the input of turbulent kinetic energy from the seiche instead of Eqs. (20) and (22) of Goudsmit et al. (2002).

$$P_{seiche} = \frac{1}{A} \cdot \frac{\partial A}{\partial z} \cdot \frac{\gamma}{\rho_W \cdot A_B} \cdot E_{seiche}^{3/2} \cdot \left(1 - 10 \cdot \sqrt{C_D}\right) . \tag{12}$$

2.5 Geochemistry

CO_2 is introduced into the lake by the sublacustrine source in the monimolimnion. At the lake surface the concentrations of CO_2 and O_2 are assumed to equilibrate with the atmosphere with an estimated gas exchange velocity of $(0.5 + 0.2 \cdot u_{10}) \cdot 10^{-5}$ m s^{-1} (MacIntyre et al. 2002). The pH is assumed to be in equilibrium with the partial CO_2 pressure and the alkalinity (defined as the sum of the positive charges of all dissolved ions). CO_2 is in equilibrium with bicarbonate and carbonate.

Dissolved iron Fe^{2+} is mixed from the hypolimnion into the mixolimnion by seasonal mixing. The operation of the degassing pipe leads to a substantial additional transport of Fe^{2+} to the surface, where it is rapidly oxidized and transformed to particulate iron hydroxide. The particles sink down with a mean velocity of

$$\rho = [999.843 + 10^{-3} \cdot (65.4891 \cdot T - 8.56272 \cdot T^2 + 0.059385 \cdot T^3)]$$
$$\times \left(\begin{array}{l} 1 + \beta_{CO_2} \cdot ([CO_2] - Alk) \cdot m_{CO_2} + \beta_{Min} \cdot (Min + m_{HCO_3} \cdot (Alk - 2 \cdot [Fe])) + \\ \beta_{Fe} \cdot [Fe] \cdot m_{FeCarb} + \beta_{part} \cdot [Fe_{Part}] \cdot m_{FePart} \end{array} \right) . \tag{11}$$

10^{-6} m s^{-1} and are quickly redissolved in the anoxic zone below the thermocline (Taillefert and Gaillard 2002).

Minerals, simulated with one state variable Min for the sum of Mg^{2+}, Ca^{2+}, K^+ and Na^+, are also introduced into the lake with the sublacustrine source and transported to the mixolimnion by diffusion and with the degassing pipe. The negative ion is mainly bicarbonate and thus included in [CO_2].

The degassing pipe transports heavy water from the monimolimnion to the surface. A large part of this buoyancy flux is lost by the degassing of the CO_2 into the atmosphere, but due to the large mineral concentrations, it nevertheless leads to a density increase in the epilimnion and below the thermocline, where the particulate iron is redissolved, and can thus potentially cause instability.

Oxygen equilibrates with the atmosphere at the surface. It is produced by primary production in the epilimnion and consumed in the sediment. Since no measurements were available, the net primary production had to be estimated at 100 g C m^{-2} a^{-1}. The concentrations of Ca^{2+} are not sufficient to lead to a supersaturation of $CaCO_3$, even when monimolimnion water with a relatively high Ca^{2+} concentration is transported to the surface waters with a pH of about 8. The precipitation of $CaCO_3$ is thus not included in the model.

2.6 Simulations

A simulation of 10 years' duration was performed with the program described above, starting on 8 November 1986, when a temperature and a CO_2 concentration profile were measured (Tietze 1987, cited in Kusakabe et al. 2000). This simulation will be referred to as the reference simulation in the following.

Sensitivity analyses were performed with 29 model parameters for all state variables – [CO_2], T, [Fe], [Fe$_{Part}$], [O_2], and Min – for the first 100 days of the simulation, which includes the convective mixing in the first dry season.

Results of the following further simulations are also presented below:

- a simulation with an additional heat input at the lake surface of 20 W m^{-2},
- a simulation with the meteorological forcing of the year 1990 repeated for 10 consecutive years,
- a simulation with the degassing pipe running for 8 months.
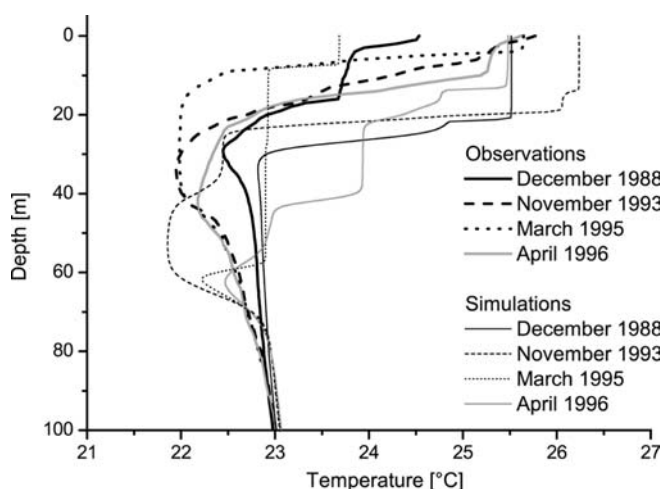
3 Results and discussion

3.1 Temperature

The annual variation of the simulated surface water temperature in Lake Nyos is small (Fig. 4). There are two similar maxima of ca. 26 °C during the wet season: the first from April to June, the second in October/November. The two minima are of different nature. The first minimum is at the end of the drier part of the wet season in August, when the surface temperature drops to ca. 25 °C. During the second minimum at the end of the dry season in January/February, the surface temperature reaches 22–24 °C, with a large interannual variability. The intensity of this second minimum is largely determined by the vapour pressure during the dry season. A low vapour pressure causes a low surface temperature due to high evaporative heat losses (Eq. 8) and lower infrared radiation from the atmosphere (Eqs. 5 and 6). A surface temperature of 22 °C is reached when the vapour pressure remains below 10 mbar for about 1 month. The simulated lake-surface temperatures are compatible with the simulation results of Kantha and Freeth (1996), who used a cyclic annual meteorological forcing, neglecting

Fig. 4 Atmospheric vapour pressure (30-day running average, *lower line*) and simulated lake surface temperature (*upper line*) from November 1986 to November 1996
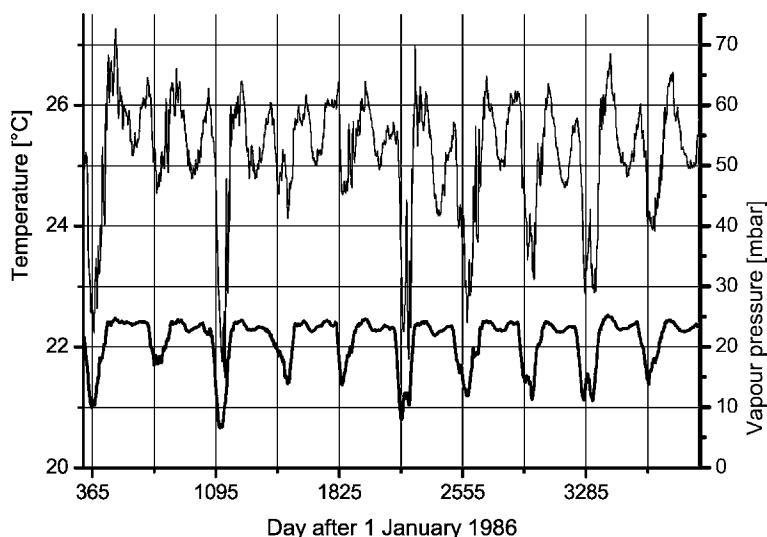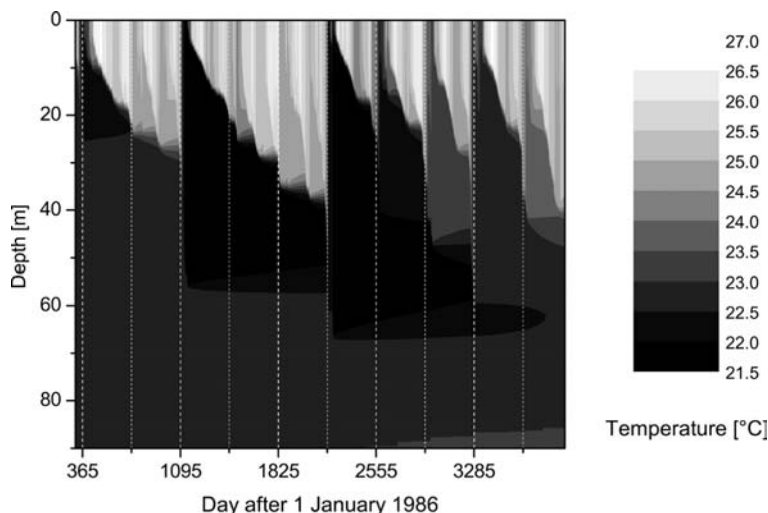
the interannual variability. An estimation of the annual minimal temperature can also be gained from observed CTD profiles (Evans et al. 1994; Kusakabe et al. 2000). These profiles show a minimum temperature at the top of the thermocline of 22 to 22.5 °C (Fig. 5). This temperature is an upper limit of the lowest surface temperature reached at the time of the last seasonal convective mixing to the given depth. The simulated temperature profiles show analogous temperature minima, but the minima are situated deeper than observed, which implies that the simulations tend to overestimate the mixing depth.

The simulated surface temperature is the most important state variable determining the depth of the mixing in the dry season. In seasons with a low surface temperature the mixing penetrates much deeper. For the simulation starting in November 1986 and ending in November 1996, these were the dry seasons at the

beginning of the years 1987, 1989 and 1992 (Fig. 6). In each of these dry seasons, the mixolimnion was deepened by about 20 to 25 m, each time preparing the ground for an even deeper mixing in the next cool dry season.

A test simulation using the meteorological forcing of the year 1990, with a relatively warm dry season, cyclically as input for a 10-year simulation, shows a regular deepening of the chemocline and a mixing depth that fits the observed CO_2 profiles well (Figs. 11 and 12). However, the annual minimal surface temperature reached in this simulation is ca. 24 °C, which means that this simulation cannot explain the low temperatures observed in the lake above the chemocline. This indicates that the parameterization of the k-epsilon model is at least partially responsible for the overestimation of the mixolimnion deepening.

The volume flow and the temperature of the sublacustrine source were assumed to be constant and adjusted to fit the observed heat increase in the monimolimnion. The best fit was achieved with a sublacustrine source of $18 \ l \ s^{-1}$ of water with a temperature of 26 °C added to the lowest meter of the water column. Evans et al. (1993) estimated a very similar temperature of the recharge water of 26.1 °C.

However, the model seems to underestimate the mixing at the lake bottom (Fig. 7). This difference between simulations and observations will be further discussed in the following section. Assuming that the water from the sublacustrine source replaces water with a temperature of 23.2 °C, the heat input to the monimolimnion by this source is $0.42 \ W \ m^{-2}$. The geothermal heat flux of $\leq 0.1 \ W \ m^{-2}$ is consequently too small to be determined by the simulations.

Fig. 5 Simulated (*thin lines*) and observed (*thick lines*) temperature profiles in the upper 100 m of the water column. The temperature minimum at 65 m depth in the simulations in 1995 and 1996 is a relic of the deep mixing in January 1992. This structure is stabilized by the salinity and CO_2 gradients

3.2 Carbon dioxide

After the eruption in 1986, the carbon dioxide concentration increased almost linearly from the monimolim-

Fig. 6 Simulated temperature in the top 90 m of the water column. Strong mixing occurred in the dry seasons in January 1987, 1989 and 1992. The *dotted vertical lines* indicate the turn of the year

nion to the surface (Nojiri et al. 1993) due to the mixing involved with the eruption. Since then, CO_2 concentrations have gradually increased in the monimolimnion, with the increase being larger in the first 2 than in later years (Kusakabe et al. 2000). On the other hand, CO_2 was lost to the atmosphere at the lake surface, building up a chemocline at the bottom of the mixolimnion. The annual mixing and the degassing led to a subsidence of the upper chemocline. The water column was thus divided into three distinctly different parts, a deepening mixolimnion with low CO_2 concentrations, a central part with almost non-changing concentrations and a growing monimolimnion with increasing CO_2 concentrations. This general behaviour is reproduced by the model.

As a consequence of the overestimation of the mixing depth (see above), the model also overestimated the deepening of the chemocline (Fig. 8). This deepening was mainly caused by the deep mixing in the cool dry seasons in 1987, 1989 and 1992 (Fig. 9), each eroding the chemocline by 20 to 25 m. The difference between the simulations and the observations could be largely explained by just one of these dry seasons not being as cool as the meteorological input data suggested.

The CO_2 concentration of the sublacustrine source was determined by fitting the parameter to reproduce the observed increases in CO_2 concentration in the monimolimnion. The observations were best predicted with an input concentration of 395 mmol l^{-1}, i.e. an annual input of 224 Mmol or 5×10^6 m^3 CO_2. The simulated input underestimates the input in the first 2 years of the simulations, and overestimates it later. This would confirm the observation of Kusakabe et al. (2000) that the CO_2 input has decreased after the first years. There is, however, also a considerable uncertainty in the CO_2 concentration profiles which were calculated from conductivity and pH measurements alone (Kusakabe et al. 2000).
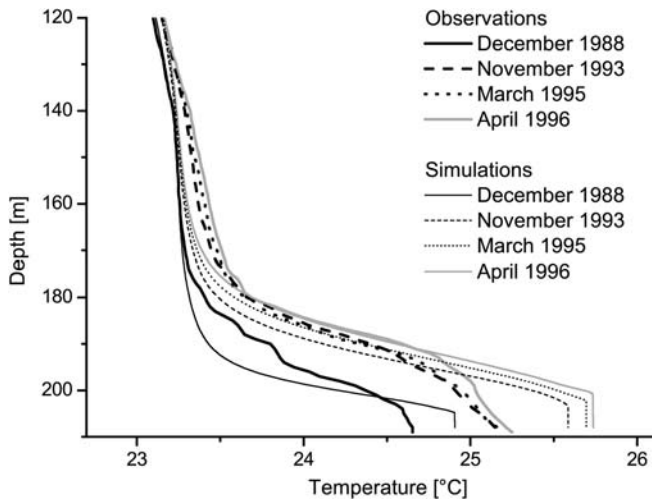
The amount of CO_2 emitted during the eruption in 1986 was estimated to 10^8–10^9 m^3 (Giggenbach 1990; Sigvaldason 1989). Since the diffusive transport through the metalimnion is several orders of magnitude lower than the input from the sublacustrine source, the CO_2 released during the eruption would be recharged within 20–200 years.

Similarly to the temperature profiles, the CO_2 profiles also indicate that the model underestimates mixing at the lake bottom (Fig. 10), but the underestimation of the mixing is smaller for CO_2 than for temperature. This difference is probably due to the fact that the molecular heat conductivity is neglected in the AQUASIM program code. Since the smallest simulated turbulent diffusion coefficients in the lower chemocline are as low as 2×10^{-7} m^2 s^{-1}, neglecting the molecular conductivity of 1.4×10^{-7} m^2 s^{-1} led to a significant underestimation of heat transport.

The following hypotheses can be set up for the underestimation of the mixing in the monimolimnion. (1) The input of turbulent kinetic energy by the seiche to the lake bottom is underestimated. (2) The sublacustrine source is located in the upper part of the monimolimnion, the heavy water plunging down to the bottom introduces kinetic energy and the detrainment of water from the plume causes some additional mixing. (3) The CO_2 and the water enter the lake separately, in which case turbulent kinetic energy could be introduced by the buoyancy flux of rising CO_2 bubbles and/or warm water. The available observed data are not sufficient to favour one of these three hypotheses.

3.3 Sensitivity analysis

The model sensitivity has been tested for 30 model parameters with the sensitivity analysis tool of AQUA-SIM (Reichert 1994). For each external time step and each grid point the error contribution (Eq. 13) was cal-
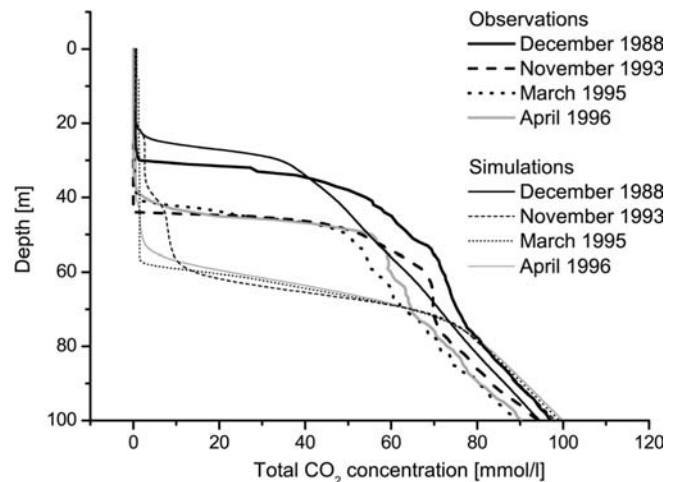
Fig. 7 Simulated and observed temperature profiles in the lower 90 m of the water column

Fig. 8 Simulated and observed total CO_2 concentrations in the upper 100 m of the water column

Fig. 9 Total CO_2 concentrations in the upper 90 m of the water column simulated from November 1986 to November 1996. The deepening of the upper chemocline occurred in three steps in January 1987, 1989 and 1992, the 3 years with the driest dry seasons
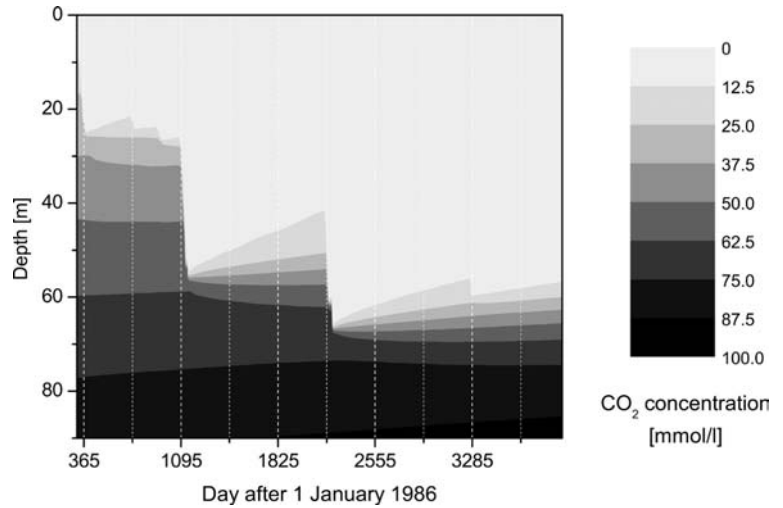
culated for every parameter p_i based on the estimated standard error σ_i for the parameter.

$$\partial_p^{\text{err}} = \frac{\partial [CO_2]}{\partial_{p_i}} \cdot \sigma_i \quad . \tag{13}$$

The root-mean-square error contribution for all grid points and time steps was calculated and normalized with the most sensitive parameter. The results are shown in Table 2 together with the standard deviations on which the calculated error contributions are based. All parameters with a root-mean-square error contribution of more than 10% compared to the most sensitive parameter p_2 are shown. The ranking of the error contributions is very similar for the other state variables. The variability of the CO_2 concentration is largest at the base of the mixolimnion, and thus the given error contributions are, in a first approximation, a measure for the sensitivity of the mixolimnion deepening to the model parameters.

Six of the seven parameters with the largest error contribution are factors which determine the surface heat fluxes. The large error contribution of the wind speed is also primarily due to its influence on the latent and sensible heat fluxes and only to a lesser extent to the surface shear stress. The only other parameter with an important error contribution is $c3_{\text{TKE}}$, which is the parameter that determines the dissipation caused by buoyancy and thus indirectly the length scale of convective mixing in the k-epsilon model. The optimal value of this parameter is a point of discussion and it has even been estimated to positive (buoyancy production reduces dissipation) and negative (buoyancy production is a source of dissipation) values for stable stratification (Burchard et al. 1998; Rodi 1980; Umlauf and Burchard 2002). The results of this study are, however, not sufficient to postulate a change of this value, because of the high sensitivity of the model to the heat fluxes.
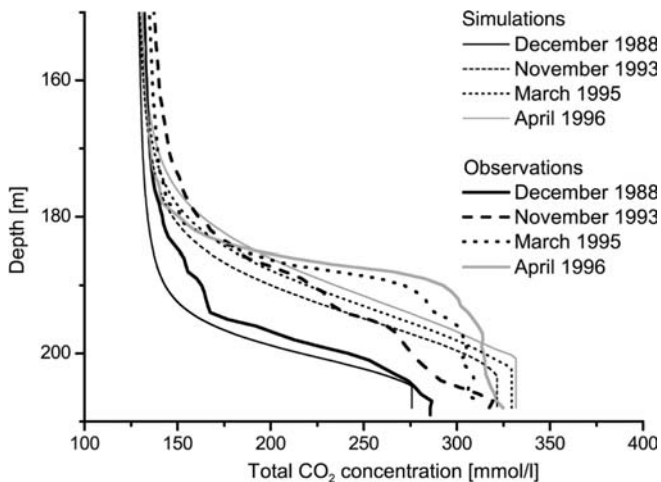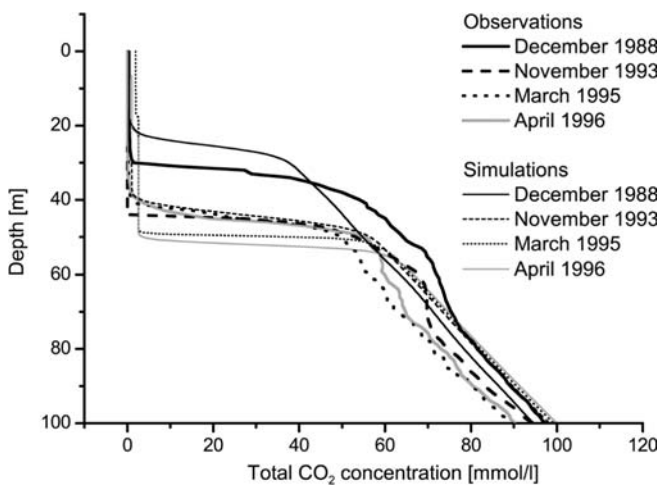

Fig. 10 Simulated and observed CO_2 profiles in the lowest 60 m of the water column

Table 2 Results of the error contribution ranking analysis of the CO_2 concentrations. The *second column* gives the value of the parameter used in the reference simulation, the *third column* the estimated standard deviation used for the error calculation, and the *last column* the root-mean-square error contribution relative to the error contribution of the most influencing parameter. All model parameters with a value >10% are shown

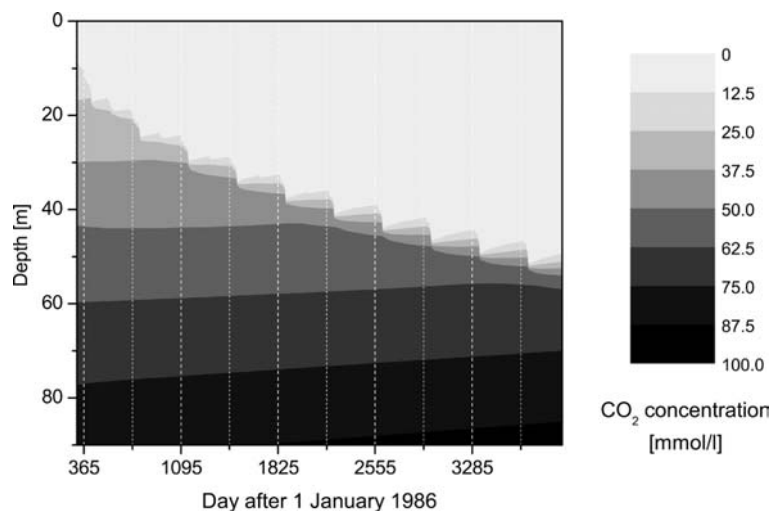| Variable	Value	Estimated standard deviation	Relative error contribution
p_2	1.0	0.2	100%
p_1	1.0	0.1	98%
u_{10}	Variable	30%	66%
$c3_{\text{TKE}}$	$B>0$: 1.0, $B<0$: −0.4	50%	59%
e_A	Variable	10%	47%
I_{ext}	Variable	5%	36%
T_{air}	Variable	0.5 °C	25%
β_{CO_2}	2.84×10^{-4} m^3 kg^{-1}	2.3×10^{-5} m^3 kg^{-1}	13%
β_I	0.4	0.1	13%
λ_0	0.4 m^{-1}	0.1 m^{-1}	12%

3.4 Degassing

First simulations of the model with the degassing pipe running have shown a subsidence of the lower chemocline of ca. 2 m within 8 months of simulation. This subsidence corresponds very well to observations made in the lake during the degassing from April to December 2001 (Fig. 13). Since the advective subsidence of the lower chemocline is caused by the sum of the discharge of the pipe of $65 \, l \, s^{-1}$ and the water input from the sublacustrine source, this observation is in agreement with the existence of a sublacustrine source and the simulated water input of $18 \, l \, s^{-1}$. The precipitation of particulate iron at the lake surface leads to a strongly reduced light transmissivity at the surface. This causes higher stability at the surface and consequently reduces the seasonal mixing depth, even though the water lifted from the monimolimnion is significantly heavier than the surface water due to the high concentrations of iron and other metal ions. For a more thorough examination of the influences of the degassing on the stratification, additional field data are needed, which will be available after the retrieval of the currently installed mooring.

4 Conclusions

The simulation model presented in this study is able to predict the general patterns observed in the CO_2 and temperature profiles of Lake Nyos. The model reproduced the development of three distinctly different layers, the deepening of the upper chemocline as well as the rise of the lower chemocline, the mixing in the monimolimnion and the almost unchanging temperatures and CO_2 concentrations in the hypolimnion.

There are, however, some quantitative differences between the model and the observations. The deepening of the mixolimnion is stronger in the model than in the observations. Since this deepening was mainly caused by three especially dry seasons with low surface temperatures, and because the sensitivity of the model to the surface heat fluxes is very high, it seems reasonable to assume that errors in the parameterization of the heat fluxes or in the meteorological forcing are the main reason for this overestimation. However, an additional simulation with only relatively warm dry seasons suggested that the parameter $c3_{TKE}$ in the k-epsilon model, which determines the mixing length scale during convective cooling, also contributes to this overestimation.

The simulated deepening of the upper chemocline of Lake Nyos is very sensitive to the heat fluxes at the lake surface. These heat fluxes depend on the meteorological forcing, especially on solar irradiation, water vapour pressure and wind speed, and on the chosen parameterization of the heat fluxes. The difference between different formulae for the heat fluxes can be as large as $50 \, W \, m^{-2}$, which would cause a difference of more than

Fig. 11 Simulated and observed CO_2 concentrations in the upper 100 m based on cyclic meteorological forcing with the data of the year 1990

Fig. 12 Simulated CO_2 concentrations in the upper 90 m based on cyclic meteorological forcing with the data of the year 1990

Fig. 13 Observed (*left*) and simulated (*right*) temperature profiles showing the deepening of the lower chemocline during 8 months of degassing with one pipe and a water flow of 65 l s^{-1}. The depths of the observed profiles were corrected for the seasonal lake level fluctuations of ≤ 65 cm
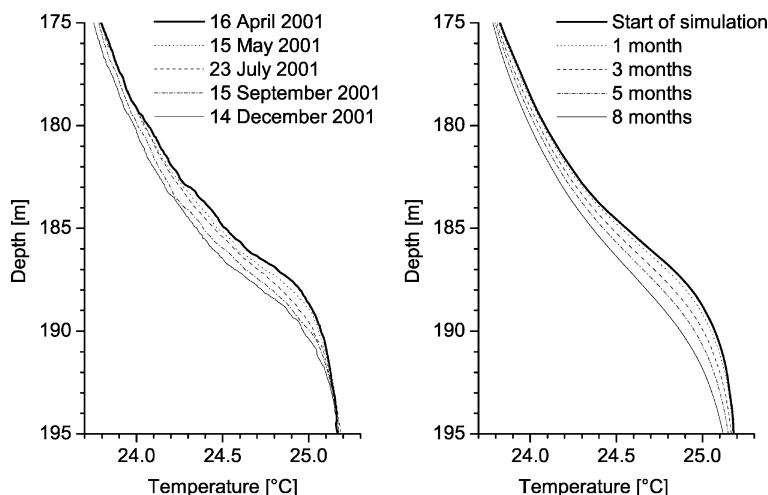
1 °C to the surface temperature. In contrast to dimictic lakes in temperate zones, where errors in the heat fluxes during summer or winter are wiped out at each seasonal overturn, an overestimation of the mixing depth in 1 year has an influence on the results of the simulation for several years or even decades. For this reason, it will not be possible to predict the meteorological forcing with sufficient accuracy for the simulation of future degassing scenarios. It will thus be necessary to set up different meteorological scenarios for the degassing calculations.

The observed increase in CO_2 and temperature at the lake bottom can be well reproduced with a sublacustrine source with a water input of 18 l s^{-1} into the monimolimnion with a temperature of 26 °C and a CO_2 concentration of 395 mmol l^{-1}. This CO_2 concentration corresponds to saturation at a depth of about 110 m. This means that without degassing, the lake would be filled up from the bottom to a depth of approximately 110 m, where the CO_2 concentration would reach saturation and a new eruption could be triggered by some sort of baroclinic dislocation. The model tends to underestimate the turbulent mixing in the bottom layers. This underestimation is larger for temperature than for CO_2, which could be explained by the fact that molecular heat conductance is not included in the AQUASIM code.

The dominant source of mixing in the mixolimnion in Lake Nyos is the buoyancy flux due to surface cooling. The buoyancy flux directly at the surface is generally positive (unstable stratification), because the lake is always near its equilibrium temperature, and since the incoming solar radiation partially penetrates the surface whereas the heat losses occur directly at the surface. Other reasons for the domination of buoyancy-driven mixing are the low wind speeds and the high thermal expansivity at the high water temperatures of more than 20 °C. Consequently, the Monin–Obukhov length, which is the depth where the turbulent energy input from wind stress is the same as from the buoyancy flux, is generally smaller than 1 m during the night. This means

that below 1 m depth the turbulence production is dominated by convection rather than wind stress. The simulated surface temperatures are lowest in December or January and thus the deep mixing occurs at that time of the year. For this reason, it seems improbable that the eruption in August 1986 could have been triggered by deep penetrative mixing, which had been one of the theories after the eruption (Kling et al. 1989). A strong baroclinic dislocation caused by a landslide or a rock fall seems to be a more reasonable candidate for the trigger of the eruption.

5 Outlook

A mooring has been installed in Lake Nyos in November 2001 with ten thermistors and four sediment traps. The high-resolution temperature time series will be used to check the simulated temperatures and to estimate the energy in the internal waves and the amplitudes of seiching at different depths. The relation of the seiching amplitudes to the vertical dislocation needed for a water parcel to reach the level of CO_2 saturation can be used as a parameter in the safety assessment.

The temperature–time series should yield more information about the reason for the underestimation of the mixing at the lake bottom. If this mixing is due to energy transfer from the seiche, higher wind speeds should cause larger vertical displacements observable in the temperature data. If the observed vertical displacements are similar throughout the year, the additional mixing is probably caused either by the sublacustrine source being at a higher elevation than the lake bottom, or by CO_2 bubbles. Recently collected CTD profiles will be used to check model simulations with the pipe running.

Finally, the model developed in this study will be used to estimate the stability of the water column for different degassing scenarios. As a consequence of the results of this study, different meteorological scenarios will be set up for the safety analysis. Furthermore, it is

also intended to use the same model for the simulation of nearby Lake Monoun, where a similar degassing procedure is currently being set up.

References

Brutsaert W (1982) Evaporation into the atmosphere: theory, history, and applications. Reidel, Dordrecht, pp 299

Burchard H, Petersen O, Rippeth TP (1998) Comparing the performance of the Mellor-Yamada and the k-ε two–equation turbulence models. J Geophys Res 103: 10543–10554

Davies JA (1965) Estimation of insolation for West Africa. Quart J Roy Meteorol Soc 91: 359–363

Davison W (1993) Iron and manganese in lakes. Earth-Science Rev 34: 119–163

Dingman SL, Weeks WF, Yen YC (1967) The effect of thermal pollution and river-ice conditions. US Army Cold Regions Research and Engineering Laboratory, Hanover, NH

Evans WC, Kling GW, Tuttle ML, Tanyileke G, White LD (1993) Gas buildup in Lake Nyos, Cameroon – the recharge process and its consequences. Applied Geochem 8: 207–221

Evans WC, White LD, Tuttle ML, Kling GW, Tanyileke G, Michel RL (1994) Six years of change at Lake Nyos, Cameroon, yield clues to the past and cautions for the future. Geochem J 28: 139–162

Gallegos CL, Moore KA (2000) Factors contributing to water-column light attenuation. In: Batiuk RA, Bergstrom P, Kemp M (eds) Chesapeake Bay submerged aquatic vegetation water quality and habitat-based requirements and restoration targets: a second technical synthesis. US EPA, Annapolis, pp 16–27

Giggenbach WF (1990) Water and gas chemistry of Lake Nyos and its bearing on the eruptive process. J Volcano Geotherm Res 42: 337–362

Gloor M, Wüest A, Imboden DM (2000) Dynamics of mixed bottom boundary layers and its implications for diapycnal transport in a stratified, natural water basin. J Geophys Res 105: 8629–8646

Goudsmit G-H, Burchard H, Peeters F, Wüest A (2002). Application of k-ε turbulence models to enclosed basins: the role of internal seiches. J Geophy Res 107: 10.1029/2001JC000954

Halbwachs M (2002) Degassing Lake Nyos project. http://perso.wanadoo.fr/mhalb/nyos/nyos.htm

Halbwachs M, Sabroux JC (2001) Removing CO_2 from Lake Nyos in Cameroon. Science 292: 438–438

Henderson–Sellers B (1986) Calculating the surface energy balance for lake and reservoir modeling: a review. Rev Geophys 24: 625–649

Huffman GJ, Adler RF, Arkin A, Chang A, Ferraro R, Gruber A, Janowiak J, McNab A, Rudolf B, Schneider U (1997) The Global Precipitation Climatology Project (GPCP) combined precipitation data set. Bull Am Meteorol Soc 78: 5–20

Imboden DM, Wüest A (1995) Mixing mechanisms in lakes. In: Lerman A, Imboden D, Gat J (eds) Physics and chemistry of lakes. Springer, Berlin Heidelberg New York. pp 83–138

Kalnay E, Kanamitsu M, Kistler R, Collins W, Deaven D, Gandin L, Iredell M, Saha S, White G, Woollen J, Zhu Y, Chelliah M, Ebisuzaki W, Higgins W, Janowiak J, Mo KC, Ropelewski C, Wang J, Leetmaa A, Reynolds R, Jenne R, Joseph D (1996) The NCEP/NCAR 40-year reanalysis project. Bull Am Meteorol Soc 77: 437–471

Kantha LH, Freeth SJ (1996) A numerical simulation of the evolution of temperature and CO_2 stratification in Lake Nyos since the 1986 disaster. J Geophys Res 101: 8187–8203

Kling GW (1988) Comparative transparency, depth of mixing, and stability of stratification in lakes of Cameroon, West Africa. Limnol Oceanogr 33: 27–40

Kling GW, Clark MA, Compton HR, Devine JD, Evans WC, Humphrey AM, Koenigsberg EJ, Lockwood JP, Tuttle ML, Wagner GN (1987) The 1986 Lake Nyos gas disaster in Cameroon, West Africa. Science 236: 169–175

Kling GW, Tuttle ML, Evans WC (1989) The evolution of thermal structure and water chemistry in Lake Nyos. J Volcanol Geotherm Res 39: 151–165

Kling GW, Evans WC, Tuttle ML, Tanyileke G (1994) Degassing of Lake Nyos. Nature 368: 405–406

Kusakabe M, Tanyileke GZ, McCord SA, Schladow SG (2000) Recent pH and CO_2 profiles at Lakes Nyos and Monoun, Cameroon: implications for the degassing strategy and its numerical simulation. J Volcanol Geotherm Res 97: 241–260

Leguern F, Shanklin E, Tebor S (1992) Witness accounts of the catastrophic event of August 1986 at Lake Nyos (Cameroon). J Volcanol Geotherm Res 51: 171–184

Lucazeau F, Lesquer A, Vasseur G (1991) Trends of heat flow density from West Africa. In: Cermák V, Rybach L (eds) Terrestrial heat flow and the lithosphere. Springer, Berlin Heidelberg New York. pp 417–425

MacIntyre S, Eugster W, Kling GW (2002) The critical importance of buoyancy flux for gas flux across the air–water interface. In: Donelan MA, Drennan WM, Saltzman ES, Wanninkhof R (eds) Gas transfer at water surfaces. AGU, Washington

McCord SA, Schladow SG (1998) Numerical simulations of degassing scenarios for CO_2-rich Lake Nyos, Cameroon. J Geophys Res 103: 12355–12364

Mitchell TD, Hulme M, New M (2002) Climate data for political areas. Area 34: 109–112

Nojiri Y, Kusakabe M, Tietze K, Hirabayashi J, Sato H, Sano Y, Shinohara H, Njine T, Tanyileke G (1993) An estimate of CO_2 flux in Lake Nyos, Cameroon. Limnol Oceanogr 38: 739–752

Ohsumi T, Nakashiki N, Shitashima K, Hirama K (1992) Density change of water due to dissolution of carbon dioxide and near-field behaviour of CO_2 from a source on deep-sea floor. Energy Conversion Management 33: 685–690

Petzold L (1983) A description of DASSL: a differential/algebraic system solver. In: Stepleman R (ed) Scientific computing: applications of mathematics and computing to the physical sciences. North Holland, Amsterdam, pp 65–68

Pickrell J (2001) Scientists begin taming killer lake. Science 291: 965–967

Reichert P (1994) AQUASIM – a tool for simulation and data analysis of aquatic systems. Water Sci Technol 30: 21–30

Reichert P (1998) AQUASIM 2.0 – User Manual. EAWAG, Dübendorf, pp 214

Rodi W (1980) Turbulence models and their application in hydraulics. International Association for Hydraulic Research, Delft, pp 104

Sigurdsson H, Devine JD, Tchoua FM, Presser TS, Pringle MKW, Evans WC (1987) Origin of the lethal gas burst from Lake Monoun, Cameroun. J Volcanol Geotherm Res 31: 1–16

Sigvaldason GE (1989) International Conference on Lake Nyos Disaster, Yaounde, Cameroon 16–20 March, 1987 – Conclusions and recommendations. J Volcanol Geotherm Res 39: 97–107

Taillefert M, Gaillard J-F (2002) Reactive transport modeling of trace elements in the water column of a stratified lake: iron cycling and metal scavenging. J Hydro 256: 16–34

Tietze K (1987) Results of the German – Cameroon research expedition to Lake Nyos (Cameroon), October/November 1986. Federal Institute for Geosciences and Natural Resources, Hannover, Germany, pp 84

Umlauf L, Burchard H (2003) A generic length-scale equation for geophysical turbulence models. J Mar Res, in press

Wüest A, Piepke G, Halfman JD (1996) Combined effects of dissolved solids and temperature on the density stratification of Lake Malawi. In: Johnson TC, Odada EO (eds) The limnology, climatology and paleoclimatology of the East African Lakes. Gordon and Breach, Toronto, pp 183–202